# Structural,Spectral and Electrical Properties of BaNi2-xZnxFe16O27 Nanoparticles Ferrites

Sadiq. H.Khoreem [1.2,*], A.H .Al-Hammadi[1],

[1] Department of Physics, Faculty of Science, Sana'a University, Sana'a, Yemen

[2] Dept. of Optometry and Vision Science, Faculty of Medical Sciences, Al-Razi University, Sana'a, Yemen

*Corresponding author: khoreems@yahoo.com

**ABSTRACT**: In the current study, w-type BNF-NPs synthesis via ceramic method.the effects of zinc ions doping on the physical properties of BNF-NPs were analyzed. The formation of BNF-NPs emphasized by XRD, FTIR, UV-Visible spectroscopy and electrical conductivity measurement. The phases structure , crysttallite size and lattice parameters wrere evaluated using XRD results. Hexagonal structure with a single phase apeares, the average grain size was found to be in Nano scale from 32 to 34 nm, while the lattice parameters increased slolly as the doping concentration of zinc ions increases. The spectra of FTIR showed main absorption bands which confirmed formation of hexagonal ferrite phase. UV-VIS analysis was also performed and found that the band gaps were in the semiconducting region and increased with increasing zinc concentration. The AC conductivity of the samples decreased with increasing zinc content and showed a dependence on the frequency and temperature. Additionally, as frequency increase the $\sigma ac$ conductivity showed dispersion that decreased as temperature increased.

CONTENTS

1. Introduction
2. Materials and Methods
3. Results and Discussion
4.Conclusion
5.References

## 1. INTRODUCTION

Investigation of ferrite nanoparticles recently became much more interesting due to the potential improvements in the physical qualities properties as well as their exceptional electrical, and optical qualities. Biosensors, recording systems, optoelectronic, catalysts, storage of data, electromagnetic resonance imaging,

ceramic layers for solar energy, optoelectronic devices, and electrical devices are only a few applications where hexa-ferrites W-type have already been extensively used. [1,2]. Due to their greater sensitivity in the optical spectrum than other varieties of materials, piezoelectric material requirements' optical characteristics have also attracted attention. Important variables to consider when researching the optical characteristics of magnetic nanoparticles which are crucial in understanding the optical properties of these materials include the absorbance value, transmittance, reflections, and the index of refraction,[3,4]. Previous research has shown that substitution of ions, such as $Zn^{2+}$ and $Co^{2+}$, can affect the magnetic properties of ferrites. For example, Ram et al. reported that substituting $Zn^{2+}$ ions, , which normally occupy at tetrahedral positions, while octahedral positions occupy by metal which have ion divalent can tailor the magnetic properties of the material, [5]. Similarly, Nakamura et al. found that the permeability and FMR frequency of Ba $(Co_{1-x}Zn_x)_2Fe_{16}O_{27}$ ferrites increased with the substitution of zinc ions [6]. For a cobalt zinc ferrite nanoparticles formulation synthesized by a ceramic procedure, Rani et al. demonstrated a reduction in the magnetic moment with raising the Zn percentage [7]. The activities of the ions of nickel and zinc it is also recognized to influences on the electrical and the material's magnetic characteristics. Zinc ions usually occupy tetrahedral positions, whereas nickel ions frequently occupy octahedral sites. As a result of these ions' interactions ions can alter the properties of ferrites. Additionally, Ferrites' characteristics are greatly influenced by their synthesis process, annealing temperature, and chemically make-up. [8–10]. In current work, researchers prepared materials of BaNiZnFe-NPs using

traditional ceramic technique. Explore performed of non-magnetic $Zn^{2+}$ ion substitution on the structure, optical behavior, and electrical conductivity of Ba-$Ni_{2-x}$-$Zn_x$-$Fe_{16}O_{27}$ with x content added from 0 to 2 by constant percent 0.4. By understanding impact ion substitution for these properties, we aim to further expand the potential applications of these materials.

## 2. Experimental & Methods

According to their molar ratio, the ceramic process was used to construct the zinc replacement barium-nickel magnetite $BaNi_{2-x}Zn_xFe_{16}O_{27}$ with constant percent from Zn from 0.0 to 2. High-purity chemical such as Barium carbonate Zinc oxides, Nickel oxide, and Iron oxide, placed in a mortar and finally ground for 3 hr to obtain dough mass. were weighed and mixed in the correct Stoichiometric ratio and grounded for six hours using an agate mortar. After that, the powder was collected in a crucible and air dried for six hours after that dried pre-sintered in oven at 950 K for 6 hours. the brown colored powder obtained was ground utilized mortar and pestle. Finally, fine powder was stocked for further characterizations. The XRD profiles were collected using XD-2 X-ray diffractometer (Beijing, China) with $CuK\alpha1$ radiation of wavelength$(\lambda) = 1.54$Å in the two-theta $(2\theta)$ degree of 5–73 and at $0.02$ $min^{-1}$. FTIR spectrum were obtained in a Nicolet iS10 spectrometer (WI, USA) at room temperature on the range of 400–4000 $cm^{-1}$. The UV-Vis spectroscopy analysis was carried out using a Hitachi PC-1650 UV-Vis spectrophotometer (Japan) on the range of 200–800 nm at RT. The electrical properties were performed on a LCR-6500P for samples sputter–coated with silver layer application.

## 3. Results and Discussion

### 3.1. XRD analysis.

The crystal phase purity for BaNiZnFeO-NPs were characterized using XRD. Fig1. displays the XRD pattern for BaNiZnFeO-NPs prepared via traditional ceramic method is shown in Figure 1. It can be deduced from the figure that the

synthesized BaNiZnFeO-NPs are in pure phase because there are no impurities observed in the XRD spectra. Additionally, it was determined via a comparison of the samples with the reference powder diffraction data from JCPDS 54-0097 that they were in good accord with the BaNi2 W-type hexaferrite structure of p63/mmc. The lattice parameters of the hexagonal structures were computed using equation (1), [11]. and the results are shown in Fig.2. It was found that both lattice constants increased with increasing zinc concentration, which can be attributed to the larger ionic radius of $Zn^{2+}$ (0.074nm) compared to $Ni^{2+}$ (0.069nm). This results in a larger distance between the ions in the lattice when $Zn^{2+}$ is substituted for $Ni^{2+}$.

$$\frac{1}{d_{hkl}^2} = \frac{4}{3}\frac{h^2+hk+k^2}{a^2} + \frac{L^2}{C^2} \tag{1}$$
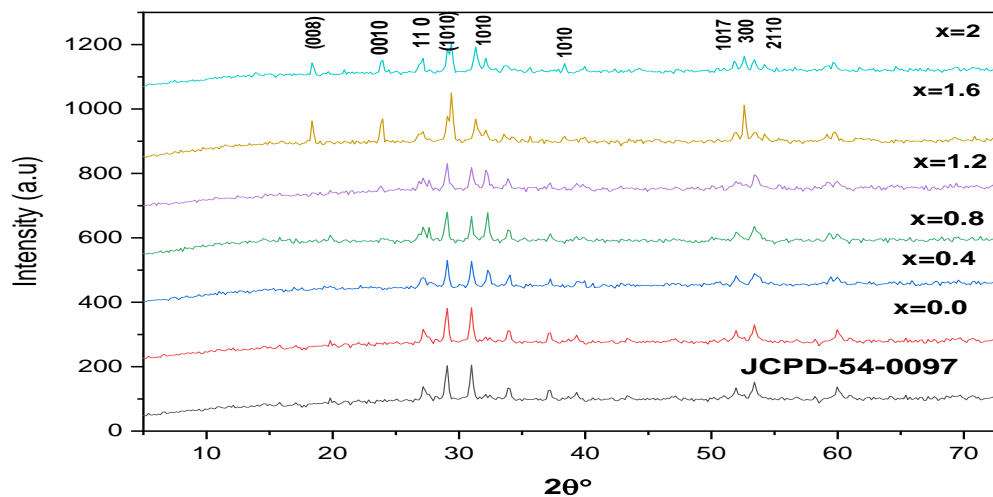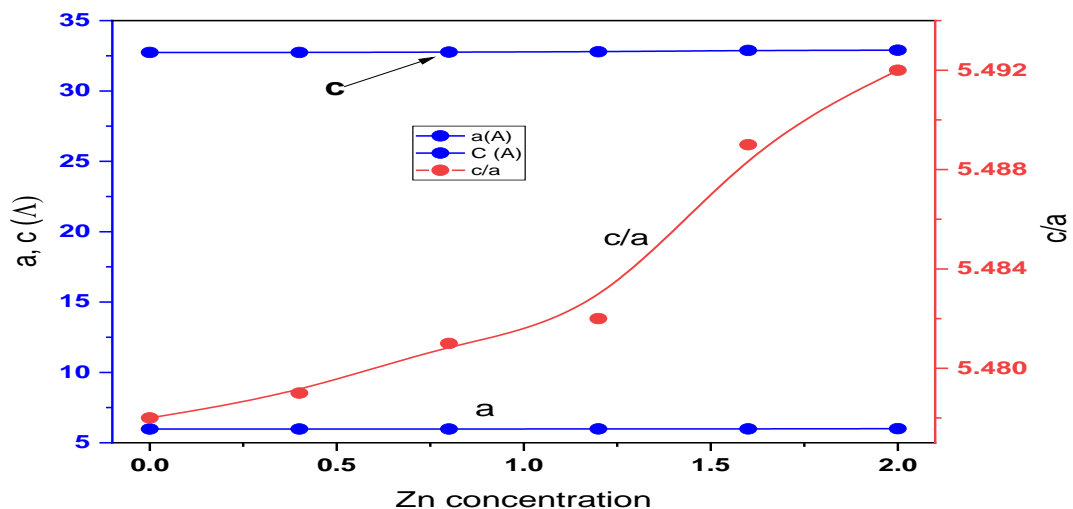


**Fig.1. Pattern of XRD for Nanoparticels BaNiZnFe16O27**



**Fig. 2. Lattice parameters (a, c and c/a) via $Zn^{2+}$ ions content of BaNiZnFe$_{16}$O$_{27}$.**

Fig.3 displays the FTIR spectrum of the BaNiZnFeO-NPs synthesized via ceramic methods. The samples display similar pattern with a little change. The peaks at 430-439.69cm$^{-1}$ and 580-595cm$^{-1}$ bonds lattice indicate the formation of hexaferrite [12]. The absorption band at 1430 and 1386 cm$^{-1}$ coincides to C-C bond at BaCO$_3$. The broad peak at 3407 is due to hydroxyl group(OH) stretching and the peak at 1643 cm$^{-1}$ is due to OH bending of adsorbed moisture in the sample and each the other peaks are attributed to the

characteristic of the material[13-14]. The absorption bands around 1624cm^{-1} and 3449cm^{-1} peaks are due to O-H stretching vibrations of water mode. The H–O–H and O–H stretching vibration at wavenumbers around 3342 cm^{-1} and 1664 cm^{-1} due to the water and polyol in the precursor [15,16]. Other peaks in the spectra are attributed to vibrations of other of H-O, and C-O, functional groups [17]. Because the large surface area of such materials, they are also attributed to bending and stretching resonance of $H_2O$ absorbed as from atmosphere when the samples were maintained and processed in the air [18]. The Peaks observed on the range of 1986–2343 cm^{-1} are instrument-based of $CO_2$ background in the sample [19]. The C-H trend is increasing is ascribed to the maximum absorption at 2900 cm^{-1} [20]. Because $Zn^{2+}$ has a lower atomic weight than its host $Ni^{2+}$ and because the wavenumber is reversed related to the atomic percent weight, the band locations $v_1-v_2$ marginally rise when x increases [21].



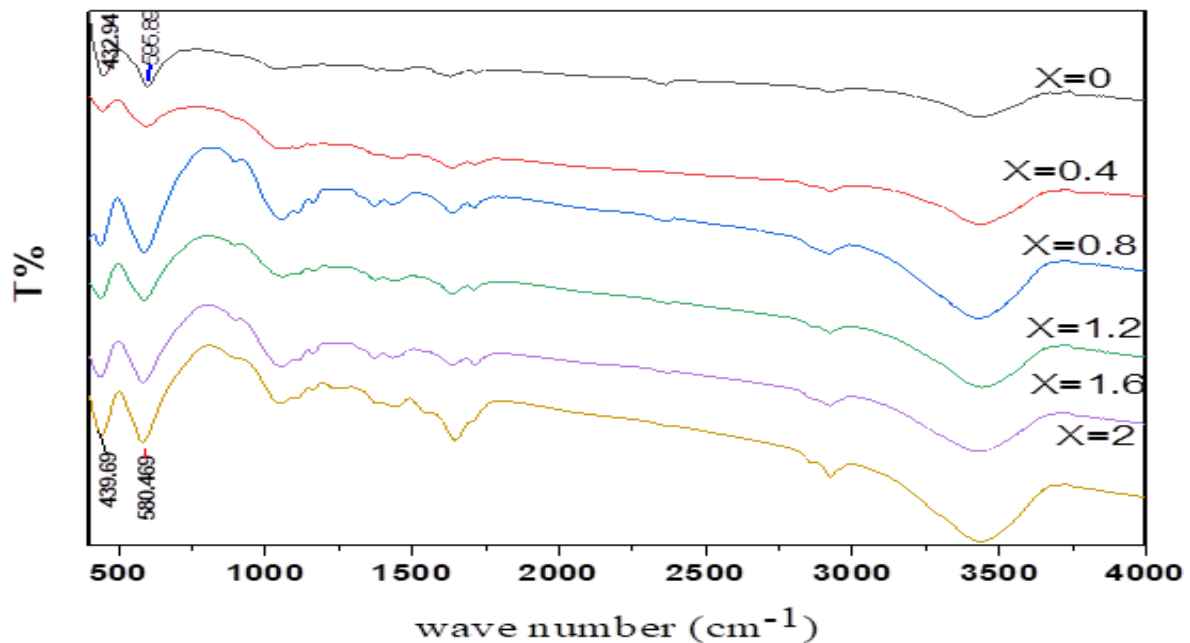**Fig. 3. IR spectra for BaNi$_{2-x}$Zn$_x$Fe$_{16}$O$_{27}$ ferrites.**

## 3.2. Optical measurements.

The optical properties for BaNiZnFeO-NPs samples were calculated at room temperature using UV–vis spectrum. The results showed that all samples were transparent at longer wavelengths (above 400 nm) and did not scatter or absorb light in the non-absorbing zone. However, at shorter wavelengths (below 400 nm), absorption caused the inequality (R+T<1) in the absorbing zone as showo in fig 4(a,b,c,d). The samples' optical transmittance margin also migrated a little amount to shorter frequencies, showing that perhaps the energy gap expanded as Zn concentration grew. All specimens' transmittance increased with increasing wavelength in the 300–400 nm region before becoming absorbed at longer wavelengths. This substance's significant 350 nm wavelength absorbance made it appropriate for use in solar cells or compounds. High transmittance was found in the infrared and the visible regions of the spectrum whereas low transmittance was

found in the ultraviolet region. As shown in Figure 3b, the Zn content increased, the optical density decreased as wavelength increases. Significant transmission was found in the infrared and the visible regions of the spectrum, while low transmission was found in the ultraviolet region. Reflectance versus wavelength in the range

of 200 nm-800 nm showed that when the percentage of Zn in the mixture rise, the reflection reduced, however the reflectivity against wavelength pattern remained largely unchanged. This showed that there was little absorbance in the near-IR and the visible regions.
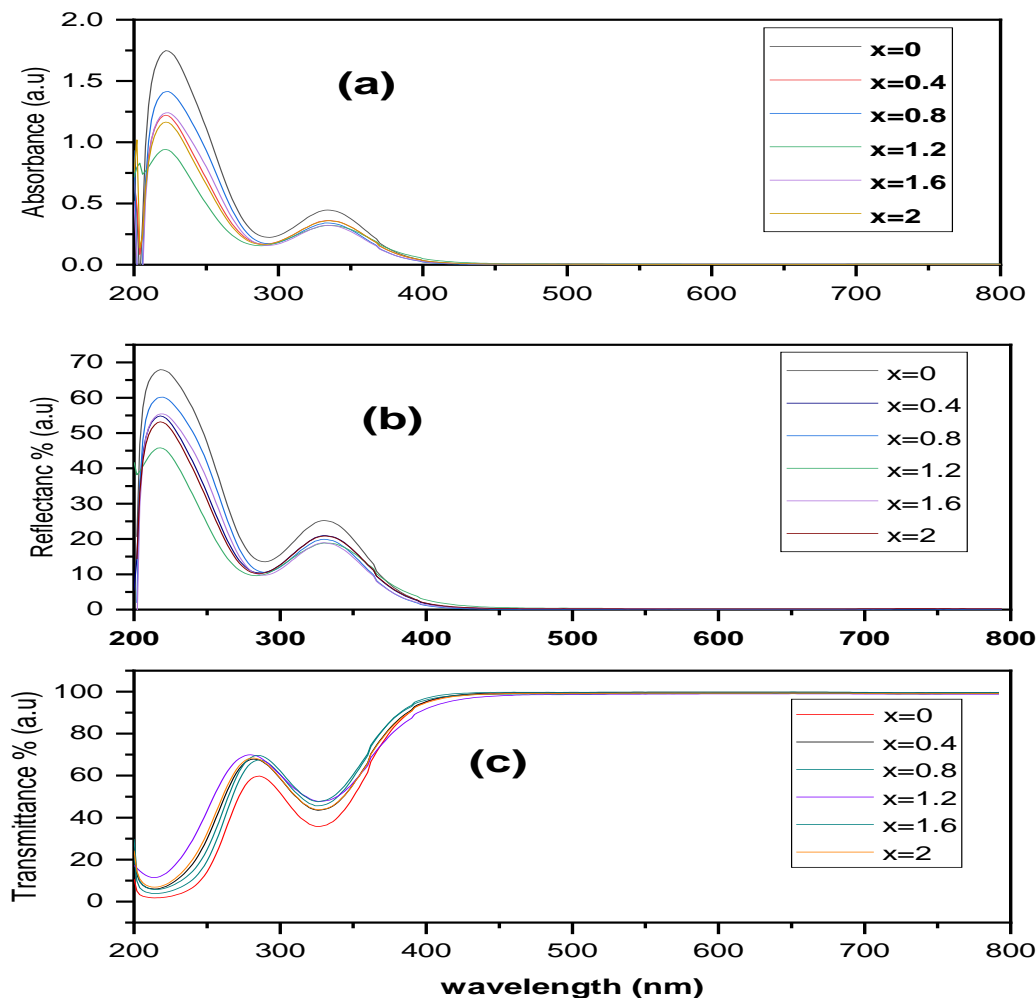


**Fig. 4. Plot of (a) Absorbance (b( Reflectance; (b) Absorbance; (c) Transmittances, versus wavelength spectra of BaNi$_{2\text{-}x}$Zn$_x$Fe$_{16}$O$_{27}$ Nnoferrite**

### 3.3 Optical bandgap.

The coefficient of absorption ($\alpha$) associated with the strong absorption region for the samples of BaNiZnFeO-NPs were computed from sample thickness(d) and absorbance (A) via equation $\alpha = 2.303A/d$[21]. The Tauc's formula ($\alpha h\nu$) =

($h\nu$-E)n, was utilized to computed optical bandgap of BaNiZnFeO-NPs [22]. The energy bandgap computed from the above data was 3.27eV to 3.37eV. In all Synthesis sample the energy bandgap was increases as the dopent concentration increases as shown in Fig.5.
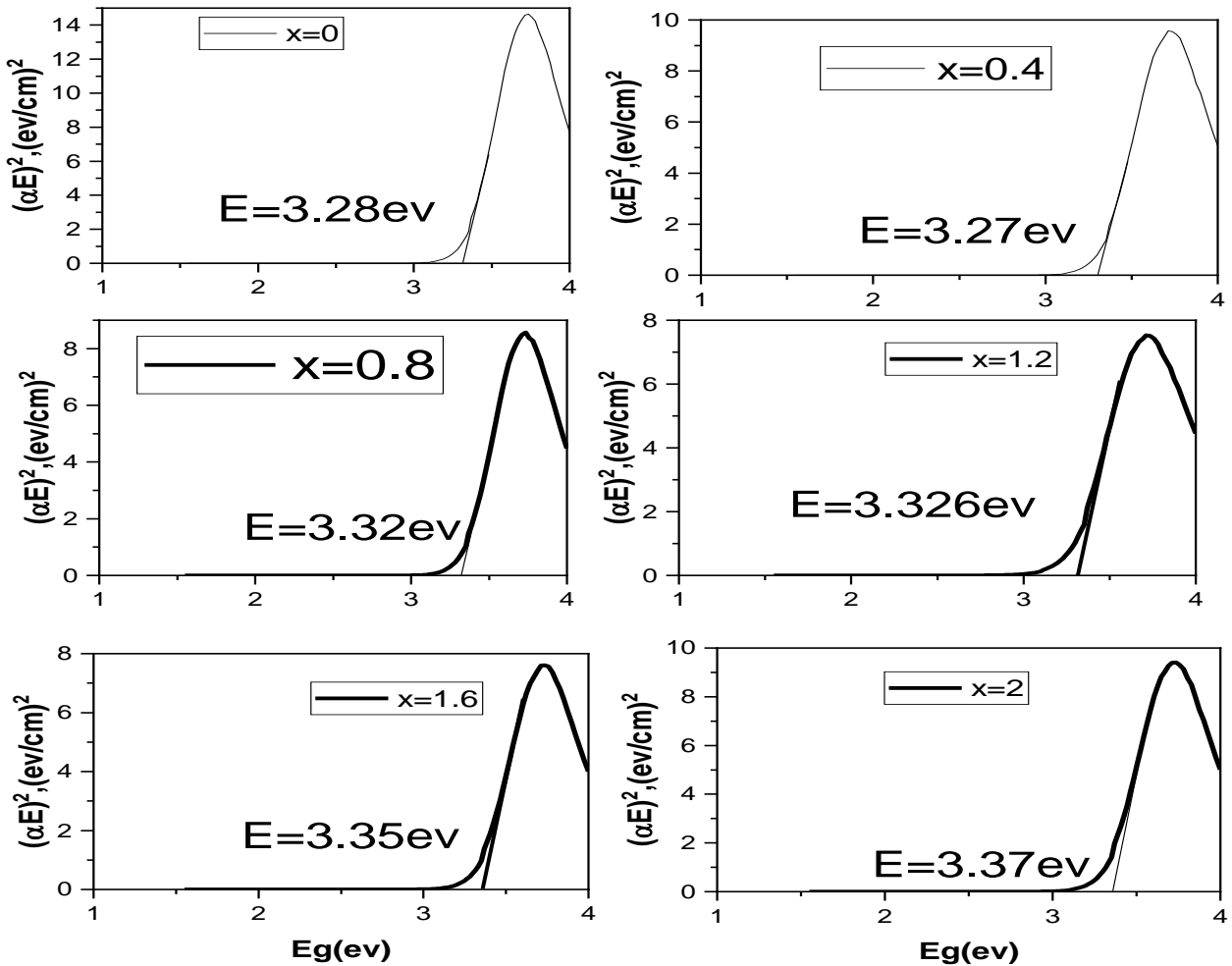
**Fig. 5. Optical energ  bandgap for  BaNiZnFeO-NPs ferrites.**

The excess in the bandgap of BaNiZnFeO-NPs with the reduce  in crystallite size might  be because of  a confinement of quantum effect. That one was revealed that the band gap increased by rising Zn2+ supply, which may have been caused by quantum confinement processes and the effect of crystallite size on Energy band gap. [23-25]. The diameter of the crystallites has really been found to have an impact on Eg, with smaller crystallites resulting in more distinct energy levels and a greater Eg. [26, 27].

## 4. Electrical Conductivity

### 4.1. Electrical Conductivity with Frequency. conductivity.

Fig.6 illustrates how the electrical conductivity (ac) of the BaNiZnFeO-NPs with percent from x start from 0.0, to 2.0. varied over frequency and at various temperatures (a,b,c,d,e,f). According to Koop's phenomenological theory[28], which holds that ferrite samples function as a multilayer inductors and suggests that the increased AC conductivity with frequency and temporal variation is caused by interfacial polarization, the results showed that the AC conductivity of all the samples

increased with rising frequency and temperature. The Maxwell-Wagner two layers model also supports this theory, [29,30], because it demonstrates that conductance is a caused by thermal process, whereby the grain boundaries are much more active at lower frequency region and the conducting grains become much more active at higher frequencies, increasing conductivity and the frequencies at which electrons among $Fe^{3+}$ and $Fe^{2+}$ ions hop. This is shown as a frequency dispersion and a linear increase in conductivity with frequency and temperature.
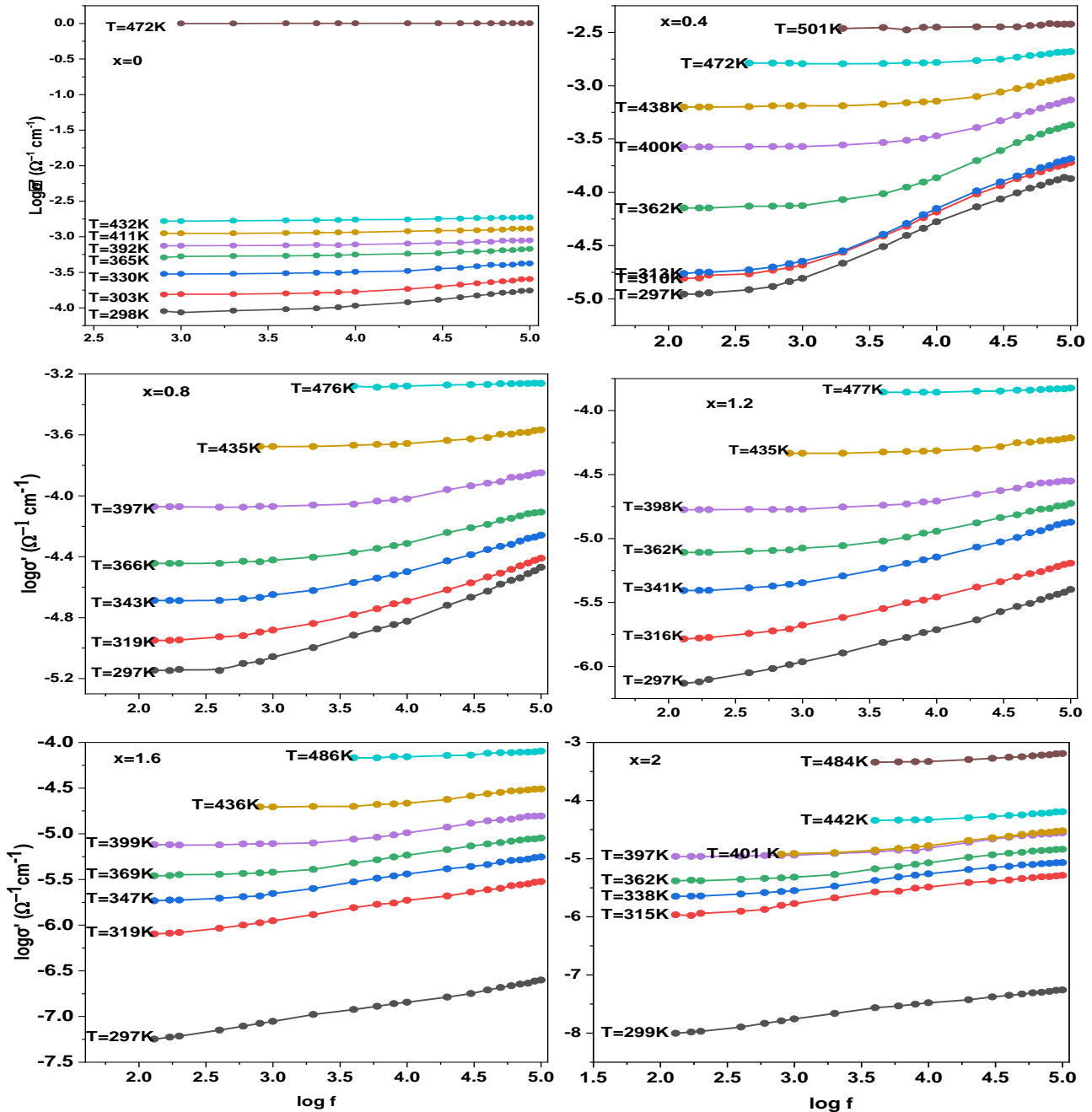


**Figure 6. Electrical conductivity for (a); $BaNi_2Fe_{16}O_{27}$ , (b):$BaNi_{1.6}Zn_{0.4}Fe_{16}O_{27}$, (c): $BaNi_{1.2}Zn_{0.8}Fe_{16}O_{27}$, (d): $BaNi_{0.8}Zn_{1.2}Fe_{16}O_{27}$, (e): $BaNi_{0.4}Zn_{1.6}Fe_{16}O_{27}$, (f): $BaZn_2Fe_{16}O_{27}$. at different temperatures.**

### 3.3.2. Electrical conductivity with temperature.

The temperature dependence of electrical ($\sigma$a.c) conductivity of the BaNi2-xZnxFe16O27 samples was also investigated. The fluctuation in ac electrical

conductivity (log ac) with the reciprocal of absolute temperature (1000/T) for various Zn contents (x) and various frequencies is depicted in Figure 7 (a, b, c, d, e, and f). The results demonstrate that the a.c. conductance revealed a semiconductor materials characteristic, increasing with rising temperature Electrical conductivity was found to be very high at high temperatures and irrespective of frequency, whereas it reduced as temperature lowered and became frequency dependent, with larger values at higher frequencies. The release of stored charges, which enhances the exchange of electrons between Fe2+ and and $Fe^{3+}$ ions, can be used to explain why electrical conductivity increases with temperature. Koop's concept and Maxwell Wagner's concept, [31–33], which propose

that in ferrite materials, the conducting grains are separated by thin layers of grain boundaries, can also explain the increase in electrical properties with temperature. The grain boundaries define the electrical conductivity behavior at low frequencies, whereas the conductivity of the grains may be responsible for the scattering at resonance voltages. A temperature dependencewas noticed in samples x=1.6 and 2, where a shift in log vs. 1000/T was established. At this temperature, the charge carriers were aligned in the field's direction due to the field and applied frequency, which increased conductivity as temperature increase. However, when the temperature was increased above Tσ, the movement of the charge carriers in various directions caused the conductivity to drop.
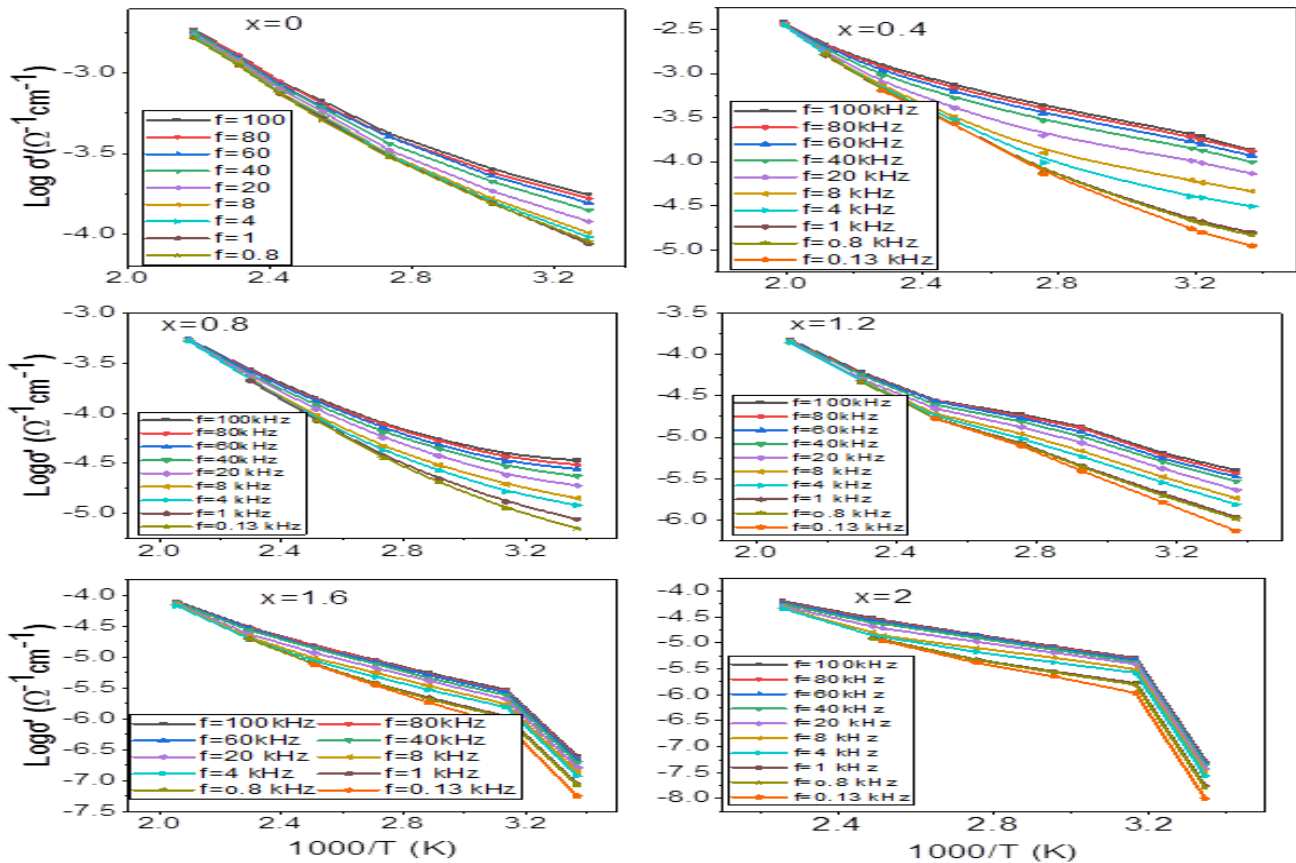


**Figure.7.(a-f). Electrical conductivity of BaNiZnFeO nanoferrites at different selected frequencies.**

## Conclusions

BaNiZnFeO-NPs ferrites have been successfully prepared using a standard ceramic methods. The X-ray diffraction pattern results indicated of single phase hexa-structure. The crystallite size and lattice parameters were also increase via increasing of zinc ions. The infra red spectra showed two primary bands of absorption are present which indicating the formation of the ferrite phase. The bandgap energy for the samples increased with increasing zinc concentration, while transmittance of samples increased as increasing wavelength at 300-400nm and then saturated at higher wavelengths. The electrical properties for samples were also affected by the substitution of Zn, with the AC conductivity increasing with both temperature and frequency. Overall, it was found that zinc replacement nickel in the $BaNiFe_{16}O_{27}$ nanoferrites produced significant modifications in the samples' electrical and optical properties, making them ideal for application, making them suitable for use in optical data storage devices.

## References

[1] Caldeira, L. E. Synthesis, Properties, and Applications of Spinel Cobalt Ferritei. In Environmental Applications of Nanomaterials. 1st ed: Springer, Cham.Switzerland AG **2022**, pp. 1-16, http://doi.org/10.1007/978-3-030-86822-2_1.

[2] Dhiman, P.; Jasrotia, R.; Goyal, D.; Mola, G.T. Hexagonal Ferrites, Synthesis, Properties and Their Applications. In book: Ferrite – Nanostructures with Tunable Properties and Diverse Applications, Materials Research Forum LLC **2021**; pp. 336-370.

[3] El Nahrawy, A. M.; Abou Hammad, A. B.; Mansour, A. M. Compositional Effects and Optical Properties of P 2 O 5 Doped Magnesium Silicate Mesoporous Thin Films. *Arabian Journal for Science and Engineering* **2021**, *46*, 5893-5906, https://doi.org/10.1007/s13369-020-05067-4.

[4] Nirmala, T. S., Iyandurai, N., Yuvaraj, S., Sundararajan, M. Third order nonlinear optical behavior and optical limiting properties of $Ni^{2+}$ ions doped zinc nano-aluminates. *Optical Materials* **2022**, *124*, 111950, https://doi.org/10.1016/j.optmat.2021.111950.

[5] You, J. H.; Kim, H. J.; Lee, J. W.; Yoo, S. I. Phase stability of $SrZnxFe_{(2-x)} Fe_{16}O_{27}$ ($0.0 \leq x \leq 1.0$) in low oxygen pressures. *Materials Science and Engineering* **2022**, *277*, 115563, https://doi.org/10.1016/j.mseb.2021.115563.

[6] Nakamura, T.; Hatakeyama, K. I. Complex permeability of polycrystalline hexagonal ferrite. *IEEE transactions on magnetics* **2000**, *36,* 3415-3417, https://doi.org/10.1109/20.908844.

[7] Rani, R.; Sharma, S. K.; Pirota, K. R.; Knobel, M.; Thakur, S.; Singh, M. Effect of zinc concentration on the magnetic properties of cobalt–zinc nanoferrite. *Ceramics International* **2012**, *38*, 2389-2394, https://doi.org/10.1016/j.ceramint.2011.11.004

[8] Kakde, A. S.; Belekar, R. M.; Wakde, G. C.; Borikar, M. A.; Rewatkar, K. G.; Shingade, B. A. Evidence of magnetic dilution due to unusual occupancy of zinc on B-site in $NiFe_2O_4$ spinel nano-ferrite. *Journal of Solid-State Chemistry* **2021**, *300*, 122279, https://doi.org/10.1016/j.jssc.2021.122279.

[9] Bera, P.; Lakshmi, R. V.; Prakash, B. H.; Devi, K.T.; Shukla, A.; Kundu, A.K.; Biswas, K.; Barshilia, H. Solution combustion synthesis, characterization, magnetic, and dielectric properties of $CoFe_2O_4$ and Co 0.5 M 0.5 $Fe_2O_4$ (M= Mn, Ni, and Zn. *Physical Chemistry Chemical Physics* **2020**, *22*, 20087-20106, https://doi.org/10.1039/D0CP03161E.

[10] Rana, G.; Dhiman, P.; Kumar, A.; Vo, D. V. N.; Sharma, G.; Sharma, S.; Naushad, M. Recent advances on Nickel Nano-ferrite: a review on processing techniques, properties and diverse applications. Chemical Engineering Research and Design 2021, 175, 182-208, https://doi.org/10.1016/j.cherd.2021.08.040.

[11] Singh, J.; Singh, C.; Kaur, D.; Narang, S. B.; Jotania, R. B.; Ateia, E.; Panina, L. Development of doped Ba–Sr hexagonal ferrites for microwave absorber applications: structural characterization, tunable thickness, absorption peaks and electromagnetic parameters. Journal of Alloys and Compounds 2021, 855, 157242, https://doi.org/10.1016/j.jallcom.2020.157242.

[12] Al-Hammadi, A.H.; Khoreem, S.H. Investigations on Optical and Electrical Conductivity of Ba/Ni/Zn/Fe16O27 Ferrite Nanoparticles. Biointerface Res Appl Chem 2022, 13, 168, http://dx.doi.org/10.33263/BRIAC132.168

[13] Ramzan, M.; Arshad, M.I.; Mahmood, K.; Amin, N.; Khan, M.I.; Iqbal, F.; Ajaz-un-Nabi, M. Investigation of Structural and Optical Properties of Pr3+-Substituted M-Type Ba–Ni Nano-Ferrites. *Journal of Superconductivity and Novel Magnetism* **2021**, *34*, 1759-1764, https://doi.org/10.1007/s10948-020-05751-4.

[14] Mosleh, Z.; Kameli, P.; Poorbaferani, A.; Ranjbar, M.; Salamati, H. Structural, magnetic and microwave absorption properties of Ce-doped barium hexaferrite. *Journal of Magnetism and Magnetic Materials* **2016**, *397*, 101-107, https://doi.org/10.1016/j.jmmm.2015.08.078.

[15] Fatima, N.; Khan, H.M.; Laref, A.; Alhashim, H.H.; Zahid, M.; Nadeem, M.; Akhtar, T.; Anjum, R. Synthesis And Characterization Of Cobalt Substituted W Type Hexagonal Ferrites. *Digest Journal of Nanomaterials & Biostructures (DJNB)* **2021**, *16*.

[16] Huang, X.; Zhang, J.; Wang, L.; Zhang, Q. Simple and reproducible preparation of barium hexagonal ferrite by adsorbent combustion method. *Journal of Alloys and Compounds* **2012**, *540*, 137-140, https://doi.org/10.1016/j.jallcom.2012.05.015.

[17] da Costa Lima, R.; Pinho, M.S.; Ogasawara, T. Thermal characterization of the intermediary products of the synthesis of Zn-substituted barium hexaferrite. *Journal of Thermal Analysis and Calorimetry* **2009**, *97*, 131, https://doi.org/10.1007/s10973-009-0256-4.

[18] Simonescu, C.M.; Tătăruş, A.; Culiţă, D.C.; Stănică, N.; Butoi, B.; Kuncser, A. Facile Synthesis of Cobalt Ferrite (CoFe2O4) Nanoparticles in the Presence of Sodium Bis (2-ethyl-hexyl) Sulfosuccinate and Their Application in Dyes Removal from Single and Binary Aqueous Solutions. *Nanomaterials* **2021**, *11*, https://doi.org/10.3390/nano11113128.

[19] Davarpanah, E.; Armandi, M.; Hernández, S.; Fino, D.; Arletti, R.; Bensaid, S.; Piumetti, M. CO2 capture on natural zeolite clinoptilolite: Effect of temperature and role of the adsorption sites. *Journal of Environmental Management* **2020**, *275*, https://doi.org/10.1016/j.jenvman.2020.111229

[20] Barbe, A.; Mikhailenko, S.; Starikova, E.; Tyuterev, V. Infrared spectra of 16O3 in the 900 - 5600 cm−1 range revisited: Empirical corrections to the S&MPO and HITRAN2020 line lists. *Journal of Quantitative* Spectroscopy *and Radiative Transfer* **2021**, *276*, https://doi.org/10.1016/j.jqsrt.2021.107936.

[21] Chavan, V.C.; Shirsath, S.E.; Mane, M.L.; Kadam, R.H.; More, S.S. Transformation of hexagonal to mixed spinel crystal structure and magnetic properties of Co2+ substituted BaFe12O19. *Journal of Magnetism* and *Magnetic Materials* **2016**, *398*, 32-37, https://doi.org/10.1016/j.jmmm.2015.09.002.

[22] Nadeem, M. S.; Munawar, T.; Mukhtar, F.; ur Rahman, M. N.; Riaz, M., Hussain, A.; Iqbal, F. Hydrothermally derived co, Ni co-doped ZnO nanorods; structural, optical, and morphological study. *Optical Materials* **2021**, *111*, 110606, https://doi.org/10.1016/j.optmat.2020.110606.

[23] Lather, R.; Jeevanandam, P. Synthesis of $Zn^{2+}$ doped $SnS_2$ nanoparticles using a novel thermal decomposition approach and their application as adsorbent . *Journal of Alloys and Compounds* **2022**, *891*, 161989, https://doi.org/10.1016/j.jallcom.2021.161989.

[24] Rajesh, K.; Sakthivel, P.; Santhanam, A.; Venugobal, J. Structural, morphological and optical behavior of $Zn^{2+}$: $CeO_2$ Nanoparticles Annealed Under Ar Atmosphere. *Romanian Reports in Physics* **2021** , *73*.

[25] Sakthivel, P.; Devadoss, I.; Krishnamoorthy, A. Band gap engineering on CdS quantum dots through dual doping of $Zn^{2+}$ and of $Ni^{2+}$ ions. *Journal of Physics: Conference Series* **2021**, *6*, 062103I, https://doi.org/10.1088/1742-6596/1964/6/062103.

[26] Terna, A. D.; Elemike, E. E.; Mbonu, J. I.; Osafile, O. E.; Ezeani, R. O. The future of semiconductors nanoparticles: Synthesis, properties and applications. *Materials Science and Engineering: B* **2021**, *272*, https://doi.org/10.1016/j.mseb.2021.115363.

[27] Kumar, N. S.; Chang, J. H.; Ho, M. S.; Balraj, B.; Chandrasekar, S.; Mohanbabu, B.; Mohanraj, K. Impact of $Zn^{2+}$ doping on the structural, morphological and photodiode properties of V2O5 nanorods. *Journal of Inorganic and Organometallic Polymers and Materials* **2021**, *31,* 1066-1078, https://doi.org/10.1007/s10904-020-01751-y.

[28] Raddaoui, Z.; El Kossi, S.; Brahem, R.; Bajahzar, A.; Valentinovich Trukhanov, A.; Leonidovich Kozlovskiy, A.; Vladimirovich Zdorovets, M.; Dhahri, J.; Belmabrouk, H. Hopping Conduction Mechanism and Impedance Spectroscopy Analyses of $La_{0.70}Sr_{0.25}Na_{0.05}Mn_{0.70}Ti_{0.30}O_3$ Ceramic. *J Mater Sci: Mater Electron* **2021**, *32*, 16113–

16125, https://doi.org/10.1007/s10854-021-06160-6.

[29] Koops, C.G. On the Dispersion of Resistivity and Dielectric Constant of Some Semiconductors at Audiofrequencies. *Phys. Rev.* **1951**, *83*, 121–124, https://doi.org/10.1103/PhysRev.83.121.

[30] Kurien, S.; Mathew, J.; Sebastian, S.; Potty, S.N.; George, K.C. Dielectric Behavior and Ac Electrical Conductivity of Nanocrystalline Nickel Aluminate. *Materials Chemistry and Physics* **2006**, *98*, 470–476, https://doi.org/10.1016/j.matchemphys.2005.08.080.

[31] Li, Z.; Senanayak, S.P.; Dai, L.; Kusch, G.; Shivanna, R.; Zhang, Y.; Pradhan, D.; Ye, J.; Huang, Y.; Sirringhaus, H.; *et al*. Understanding the Role of Grain Boundaries on Charge-Carrier and Ion Transport in $Cs_2AgBiBr_6$ Thin Films. *Adv. Funct. Mater.* **2021**, *31*, 2104981, https://doi.org/10.1002/adfm.202104981.

[32] Mazen, S.A.; Abdel-Daiem, A.M. IR Spectra and Dielectric Properties of Cu–Ge Ferrite. *Materials Chemistry and Physics* **2011**, *130*, 847–852, https://doi.org/10.1016/j.matchemphys.2011.09.017.

[33] Ahmad, I.; Shah, S.M.; Zafar, M.N.; Ashiq, M.N.; Tang, W.; Jabeen, U. Synthesis, Characterization and Charge Transport Properties of Pr–Ni Co-Doped $SrFe_2O_4$ Spinel for High Frequency Devices Applications. *Ceramics International* **2021**, *47*, 3760–3771, https://doi.org/10.1016/j.ceramint.2020.09.233

[34] Al-Hammadi, A.H.; Khoreem, S.H. Impact of Zinc Substitution on AC Conductivity Behaviors of Hexagonal Ba-Ni Ferrite Nanoparticle. Biointerface Res Appl Chem. 2022, 13, 364, https://doi.org/10.33263/BRIAC134.364